Energy Reports 8 (2022) 3011–3017

Contents lists available at ScienceDirect

Energy Reports

journal homepage: www.elsevier.com/locate/egyr

Research paper

Analytical design of a radial-flux PM generator for direct-drive wind turbine renewable energy application

Reza Yazdanpanah [a], Abdolkarim Afroozeh [a,*], Mahdiyeh Eslami [b]

[a] Department of Electrical Engineering, University of Larestan, Lar, Iran
[b] Department of Electrical Engineering, Kerman Branch, Islamic Azad University, Kerman, Iran

ARTICLE INFO

Article history:
Received 12 October 2021
Received in revised form 10 January 2022
Accepted 16 January 2022
Available online 18 February 2022

Keywords:
Direct-drive
PM generator
Renewable energy
Wind turbine

ABSTRACT

Renewable energy resources have attracted the attention of the power generation industry in recent years as they have no pollution and the advantage of unlimited energy harvesting. One of these resources is the wind that is available in most areas of the world. Electrical energy generation from wind power requires suitable generators that different types and systems have been studied in the literature. In this study, the design of a 1 kW, 50 Hz, and 500 RPM permanent magnet generator using analytical electromagnetic fields analysis is presented that is based on the initial requirements of a wind power generation system. Also, performance analysis of the designed generator of simulations using the finite element approach has been investigated. The simulation results of the generator characteristics including, output voltage and power verifies the initial design constraints and required performances. The novelty of this study investigates the design and performance characteristic analysis of a radial-flux PM generator for wind power generation application.

1. Introduction

As the conventional sources of energy are reducing, renewable energy has an important role in the future energy market. In many regions of the world, the wind is powerful enough to provide the mechanical energy of wind generators. To extract electric energy from wind, it is first converted into kinetic of turbines and then electrical energy by using different types of low to medium power generators. The generator is connected to the turbine and load. The operating speed range of the wind power generators for the average wind speed of 3–5 m/s, is 100–500 rpm (Dobzhanskyi et al., 2019).

For the advancement of electrical machines, material technology is of great importance. For example, permanent magnets (PM) in electrical machines, and in particular rare-earth PMs with high energy densities, have greatly improved efficiency, reliability, and power density. The high power density of PM machines makes them potential candidates for direct-drive applications. Various topologies of PM machines (PMM) with a large number of poles are characterized as high torque density and efficiency machines (Yang et al., 2020; Yazdanpanah and Mirsalim, 2014; Gieras, 2002; Zhao et al., 2019; Chen et al., 2020). So, PMMs are used in low-speed and high torque applications such as direct-drive wind and hydropower turbines, long-stroke application, propulsion systems, and electric vehicles (Husain et al., 2018; Dincer and Acar, 2015; Şahin et al., 2006; Elizondo et al., 2009; Li et al., 2021a).

While reluctance motors may be alternatives to the PMM (Li et al., 2021b), their performance in terms of high power density, high efficiency, and low torque pulsation is not as good as the PMMs (Zhao et al., 2021). In spite of the fact that the PM synchronous generator (PMSG) is a well-established solution for wind power generation, the PM field in PMSG is difficult to adjust, which limits its speed range. Compared to the mechanical gear-down operation, this machine produces high torque at low speeds, which is highly suitable for low-speed motoring and generating applications. While the addition of PMs to the rotor enhances torque and power density, lower power factor at the stator terminal is still undesirable because of harmonic leakage in the air gap (Du and Lipo, 2017).

PMM with hybrid PMs is proposed to increase the output characteristics and reliability (Jeong et al., 2019). By utilizing unused space within a machine structure, the hybrid excitation structure can effectively increase torque density. Besides the PM, the winding is an important part of the PMMs and plays a key role in reliability (Li and Cheng, 2020). In recent developments of PMMs, torque density has improved, but the choice of PM has yet to be considered with an aim to reduce the material cost. Moreover, the issue of demagnetization for the PMs in cases of faults has not been resolved. Another challenge is the unbalanced force in the PMM, which causes bearing life to be shorter, vibrations,

* Corresponding author.
E-mail address: afroozeh@lar.ac.ir (A. Afroozeh).

https://doi.org/10.1016/j.egyr.2022.01.121

and noise to occur. PM materials have different characteristics and properties that could be summarized as follows. Ferrite magnets have a low cost, but low energy product and mechanical strength. The mechanical strength and cost of Alnico are high on the other hand, its energy product is low. The advantage of SmCo is its high energy produced while the disadvantages are high cost and low mechanical strength. Finally, NdFeB is the most powerful in terms of energy nevertheless, its cost is high and mechanical strength is low. Various topologies are introduced and discussed in relation to the machine structure for direct-drive applications. Axial-flux PM machines have the advantages such as compact structure, high aspect ratio, planar structure, and short axial length (Li et al., 2019). The PM linear machines have been extensively researched and applied to linear direct-drive applications and to high-precision servo motors (Gao et al., 2017). They separate armature winding and magnetic poles, respectively, into the primary and secondary. Due to the high use of rare earth PMs in long-stroke applications, the cost is extremely high (Shen et al., 2021). Transverse flux PM machines have become popular due to the use of lower strength ferrite magnets. However, they suffer from high leakage flux and high inductance, which lead to low power factor, high core loss, and saturation, and on top of that, it is difficult to construct (Chowdhury and Sozer, 2020). Rotating structures of both axial and transverse flux PM machines have complex 3-dimensional magnetic flux paths, compared to the traditional radial flux machines (Feng et al., 2018). Additionally, as these topologies are difficult to construct from lamination iron, their core material has a lower permeability and saturation flux density. As a result, radial flux PM machines are more suitable for analytical design studies in which the field variables are 2-dimensional.

Due to higher efficiency and lower noise and vibration, direct-drive wind turbines are preferred, where by eliminating the gear box, turbine maintenance reduces which is important for offshore applications (Nasiri-Zarandi et al., 2020; Alhmoud and Wang, 2018; Zhang et al., 2017). In other words, higher power rating wind turbines work at lower speeds. In this paper, a 1 kW, 500 rpm radial flux PM generator is designed to be used in a direct-drive wind power generation. The design and analysis of electrical machines are based on analytical and numerical calculations of electromagnetic field variables. The performance analysis can be achieved by the numerical methods, but the analytical equations can facilitate the design procedure (Hong et al., 2018).

The novel aspect of this study pertains to the design and evaluation of a radial-flux PM generator that can be applied to wind power generation. Contributions of this study include presenting a new analytical model of the radial-flux PMM with buried PMs as well as sizing and design equations based on the electromagnetic field analysis. This approach is applicable for design and manufacturing the PMM of other specifications and applications.

The rest of the paper is organized as follows: Section 2 presents a description of the wind power generator design. The analysis and analytical design equations of the generator considering the requirements and design constraints are included in this section. The simulation results of the generator performance and characteristics, including magnetic flux analysis and voltage and power characteristics in no load and loading conditions are presented in Section 3. Finally, the conclusions are drawn in Section 4.

2. Generator design

Synchronous generators are the main source of electricity by converting the mechanical output power of steam and gas turbines, reciprocating engines, and water turbines into electrical power. Some wind turbine designs also, use this type of generator. In terms of energy use, a high-power wind power generator connected to the grid is currently one of the most effective ways to use wind energy. This system converts wind energy into mechanical energy by wind turbines and then into electrical energy by the generator. Therefore, direct-drive power technology with the ability to track the maximum wind PowerPoint at wind speed has become one of the hot spots in the studies. The direct-drive wind power generation system is shown in Fig. 1. The nominal power of the wind turbine and its speed are related as shown in (1) (Nasiri-Zarandi et al., 2020).

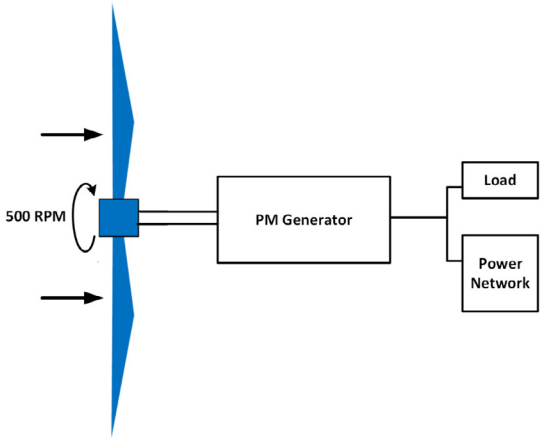

Fig. 1. Direct drive wind power generation system.

Table 1
Wind power generator initial parameters.

Parameter	Value
Output power	1000 watt
Output voltage	220 V
Speed	500 RPM
Frequency	50 Hz

$$\omega_r \propto \mathbf{P}^{-0.5} \tag{1}$$

That is, higher power wind turbines have lower speeds.

2.1. Generator topology and specifications

The inner rotor radial flux PM generator is designed and analyzed in this study with the topology and elements shown in Fig. 2. The stator is composed of laminated core and windings. The rotor is made of a laminated core in which the PMs are inserted. Based on the wind generator requirements and (1), the specifications of the generator are reported in Table 1.

2.2. Rotor and stator design

The generator power and main geometrical parameters are related to each other as:

$$\mathbf{P} = C_0 D_o^2 L \omega \tag{2}$$

Where, $\mathbf{P}$ is the power, D_0 and L are the diameter and axial length, respectively, ω is the rotational speed and C_0 is (Pyrhonen et al., 2013; Hanselman, 2003):

$$C_0 = 10.9624 \times B_{av} \times ac \times k_{sw} \tag{3}$$

Where, B_{av} and are ac the magnetic and electrical loadings and k_{sw} is the winding factor.

So, for the selected diameter to length ratio, these parameters are calculated using (2) and Table 1.

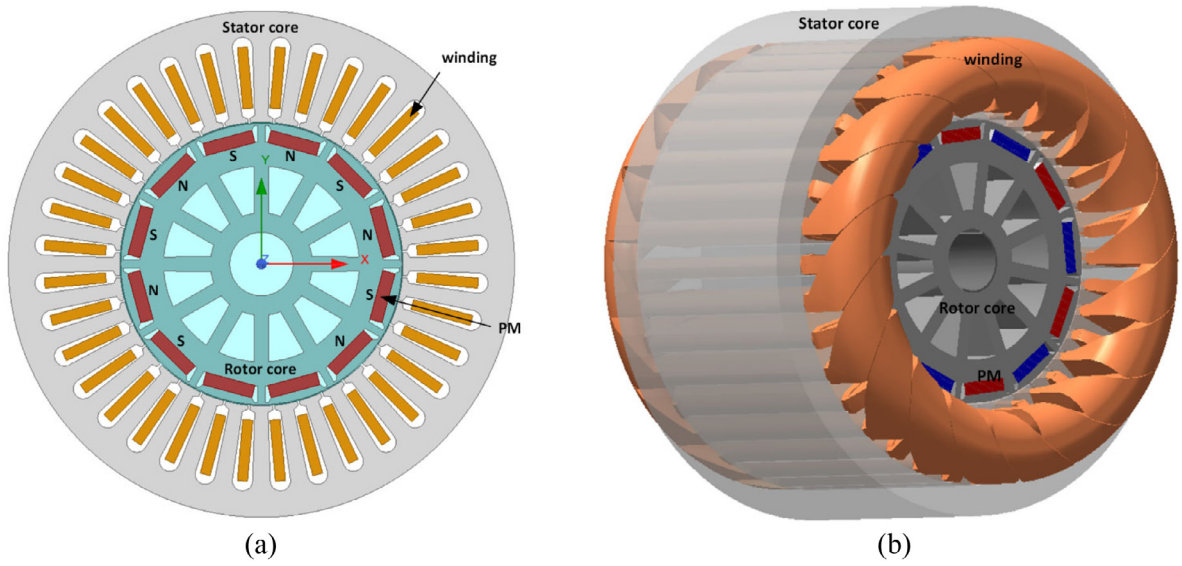

Fig. 2. Radial flux PM generator structure, (a) 2D view, (b) 3D structure.

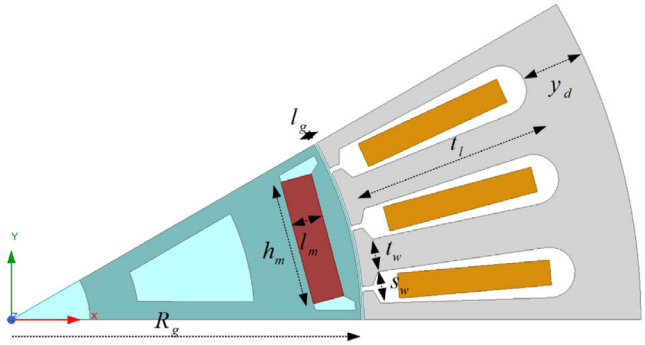

Fig. 3. Geometrical parameters.

Fig. 3 shows a section of rotor and stator. Assuming no flux leakage when the flux crossing the air-gap to the stator teeth:

$$s.A_tB_t = A_gB_g \rightarrow s.t_wK_{st}LB_t = 2\pi R_gLB_g \rightarrow t_w = \frac{2\pi R_gB_g}{s.K_{st}B_t} \quad (4)$$

Where, A_t, A_g, B_t and B_g are the tooth and air-gap area and magnetic flux density, respectively. R_g is the average air-gap radius and K_{st} is the lamination fill factor of the core, and s is the slot number.

Assuming the half of magnetic flux crossing the stator yoke:

$$s.B_{sy}K_{st}L.y_d = \pi R_gLB_g \rightarrow y_d = \frac{\pi R_gB_g}{s.K_{st}B_{sy}} \quad (5)$$

In (4) and (5), B_t and B_{sy} are the maximum permissible flux density of the core that depends on the used magnetic material.

Similar method is used to find the rotor yoke depth.

The magnetic equivalent circuit (MEC) of the flux path is shown in Fig. 4a (Yazdanpanah, 2020). In this figure, R_g, R_m and R_l are the air-gap, PM and leakage reluctances, respectively. ϕ_r is the PM residual flux. As the leakage reluctances are large, this MEC could be simplified to Fig. 4b.

From Fig. 4:

$$\phi_g = \frac{R_m}{R_m + R_g}\phi_r \quad (6)$$

Where:

$$R_m = \frac{l_m}{\mu_0\mu_r h_m L}, R_g = \frac{l_g}{\frac{2\mu_0\pi R_gL}{p}} \quad (7)$$

Where,

p is number of poles.

(6) Results in:

$$A_gB_g = \frac{R_m}{R_m + R_g}A_mB_r \rightarrow B_g = \frac{R_m}{R_m + R_g}\frac{A_m}{A_g}B_r \quad (8)$$

Selecting the air-gap flux density and the fringing effect factor ($\frac{A_m}{A_g} = C_\phi$), h_m is calculated as:

$$\frac{A_m}{A_g} = \frac{h_mL}{\frac{2\pi R_gL}{p}} = C_\phi \rightarrow h_m = C_\phi\frac{2\pi R_g}{p} \quad (9)$$

And considering Fig. 4b:

$$l_m = \frac{\phi_g\left(R_m + R_g\right)\mu_0}{B_r} \quad (10)$$

2.3. Winding design

The induced voltage could be calculated by Jeong et al. (2019), Li and Cheng (2020):

$$E = 4.44Nf\phi_g \quad (11)$$

Where, N is number of turns, f is frequency and ϕ_g is the per pole flux that is calculated by:

$$\phi_g = \frac{A_gB_g}{p} = \frac{2\pi R_gLB_g}{p} \quad (12)$$

Considering the rated power, rated current is:

$$I = \frac{\mathbf{P}}{3.\eta.V.\cos\varphi} \quad (13)$$

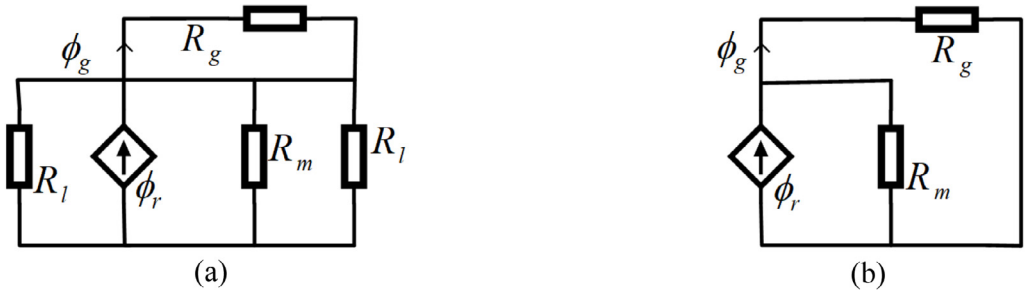

Fig. 4. MEC, (a) detailed, (b) simplified.

winding type: Lap
number of coils per slot: 1
coil span: 3
number of layers: 1

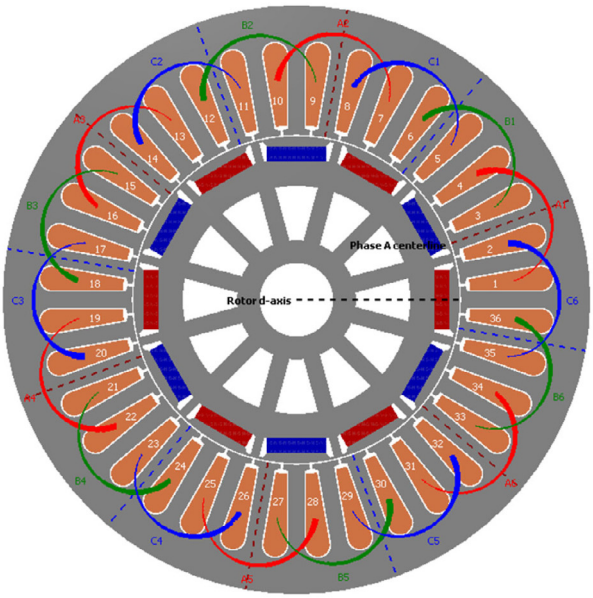

Fig. 5. Winding configuration.

So, based on the cooling system and the selected current density (J), the conductor area and diameter are calculated:

$$A_w = \frac{I}{J} \tag{14}$$

$$d_w = \sqrt{\frac{4A_w}{\pi}} \tag{15}$$

2.4. Designed generator

Considering design equations and selected design parameters, the designed generator has the parameters reported in Table 2.

3. Simulation results

In this section, the designed generator is simulated by the finite element analysis (FEA) to investigate the output characteristics. The core material is M-400 and the PM residual flux density is 1.08 T. Fig. 5 shows the winding configuration and the mesh grid is shown in Fig. 6.

To reduce the simulation cost and time, master and slave boundary condition is used to simulate only one pole of the machine structure. So, the mesh structure shown in Fig. 6a is applied to overall geometry including the air-gap.

Table 2
Designed generator parameters.

Parameter	Symbol	Value
Number of phase	N	3
Number of poles	p	12
Number of stator slots	s	36
Air-gap length	l_g	0.5 mm
Air-gap mean radius	R_g	55.75
Outer diameter	D_o	200 mm
Axial length	L	100 mm
PM length	l_m	5 mm
PM height	h_m	20 mm
Tooth width	t_w	5.5 mm
Tooth length	t_l	32 mm
Stator yoke length	y_d	10 mm
Fill factor	K_{st}	0.43
Current density	J	3.5 A/mm^2
Rated torque	T	19.1 N m

To enhance the calculation accuracy, mesh of the geometry is refined especially in the narrow parts and where the flux path and direction change. The refinement is divided into 3 different

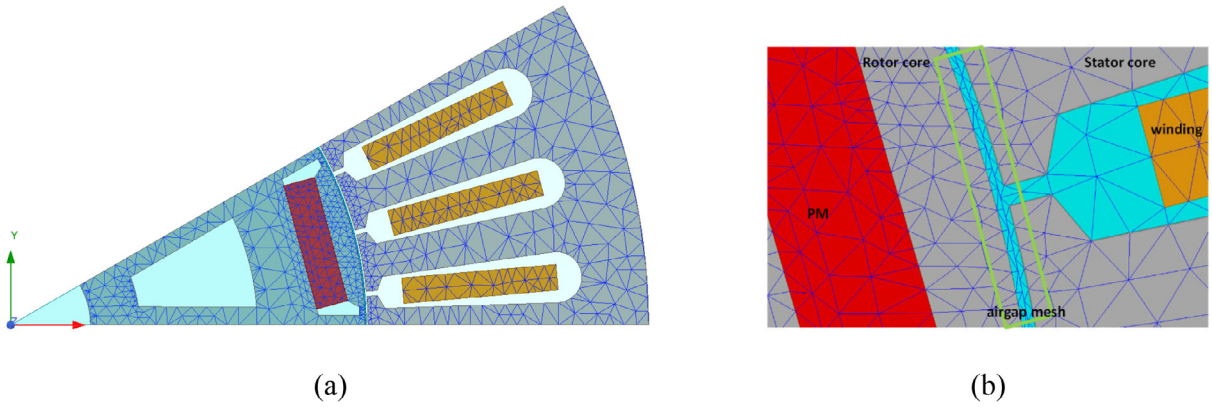

Fig. 6. Mesh grid, (a) a section of the generator, (b) air-gap mesh.

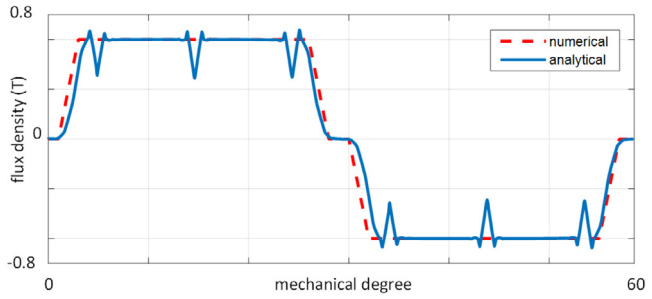

Fig. 7. Magnetic flux density in the air-gap.

sections: the stator and rotor cores, the PMs, and the coils. Considering the geometry, maximum element lengths of the sections are selected as 3 mm, 1 mm, and 2 mm, respectively. The air-gap mesh is shown separately in Fig. 6b.

To compare the analytical and numerical calculations of air-gap magnetic flux density, the results are shown in Fig. 7. The discrepancy between the results is caused by the stator teeth and slot openings that their actual shapes are not considered in the analytical model.

3.1. No load test

The generator is simulated in no load condition at the rated speed, where the flux distribution in different parts is shown in Fig. 8. The flux density in the core is about 1.7 T that is lower than the saturation limit.

Fig. 8a shows the magnetic flux density distribution in different part of the stator and rotor core to ensure the saturation prevention. It shows one fourth of the machine's structure (3 poles) and the same applies to the rest of it. Moreover, the flux lines and the flux paths are illustrated in Fig. 8b as well as the magnetic vector potential.

In PM rotors, short circuiting flux is the main problem. The flux barriers in the rotor structure improve the flux lines passing through the air-gap due to decreasing the short circuiting flux. In other words, the placement of the flux barrier at the rotor, results in a more uniform distribution of flux density as shown in Fig. 8c.

The cogging torque of the generator is an important parameter that is due to the interaction between PMs and the teeth. In the designed generator, Fig. 9 shows that the cogging torque is about 1.8 N m and less than the 10% of the rated torque. As a result of nonlinear characteristics of the machine, torque ripple varies at different operating conditions that results in complexity in computation and analysis. The cogging torque could be decreased by techniques like rotor or stator skewing, slot opening adjustment, fractional slot windings, bifilar teeth, etc. (Yazdanpanah and Farjah, 2021; Liang et al., 2019).

Table 3
Generator Loss.

Loss component	Value
Copper loss	78 watt
Core loss	15 watt
Total	93 watt

Back-EMF and its harmonics content are shown in Fig. 10. It is clear that only the 7th and 11th component have considerable magnitude.

3.2. Loading test

The output power at different speeds is shown in Fig. 11 varying load impedance. In this figure, the output power at rated speed is about 1 kW that is specified in Table 1.

Fig. 12 Compares the no load and loading voltages of the generator. The RMS value of the voltage is 220 V as specified in Table 1.

3.3. Losses and efficiency

In this generator, loss is composed of copper, core and mechanical losses. Ignoring the mechanical loss, the copper and core losses could be calculated based on the FEA of the generator at the rated speed and power as presented in Table 3.

So, the efficiency is calculated as the output power to the sum of output and loss power as:

$$\eta = \frac{\mathbf{P}}{\mathbf{P} + loss} \simeq 92\%$$

3.4. Sensitivity analysis

The output line voltage for different air-gap length and PM thickness is shown in Figs. 13 and 14, respectively. Fig. 13 shows that the smaller air-gap length increases the produced output voltage. Nevertheless, this length is limited by mechanical considerations.

From Fig. 14 it can be concluded that the PM thickness has no significant effect on the output characteristics. This is due to the negligible effect of this parameter on the air-gap flux.

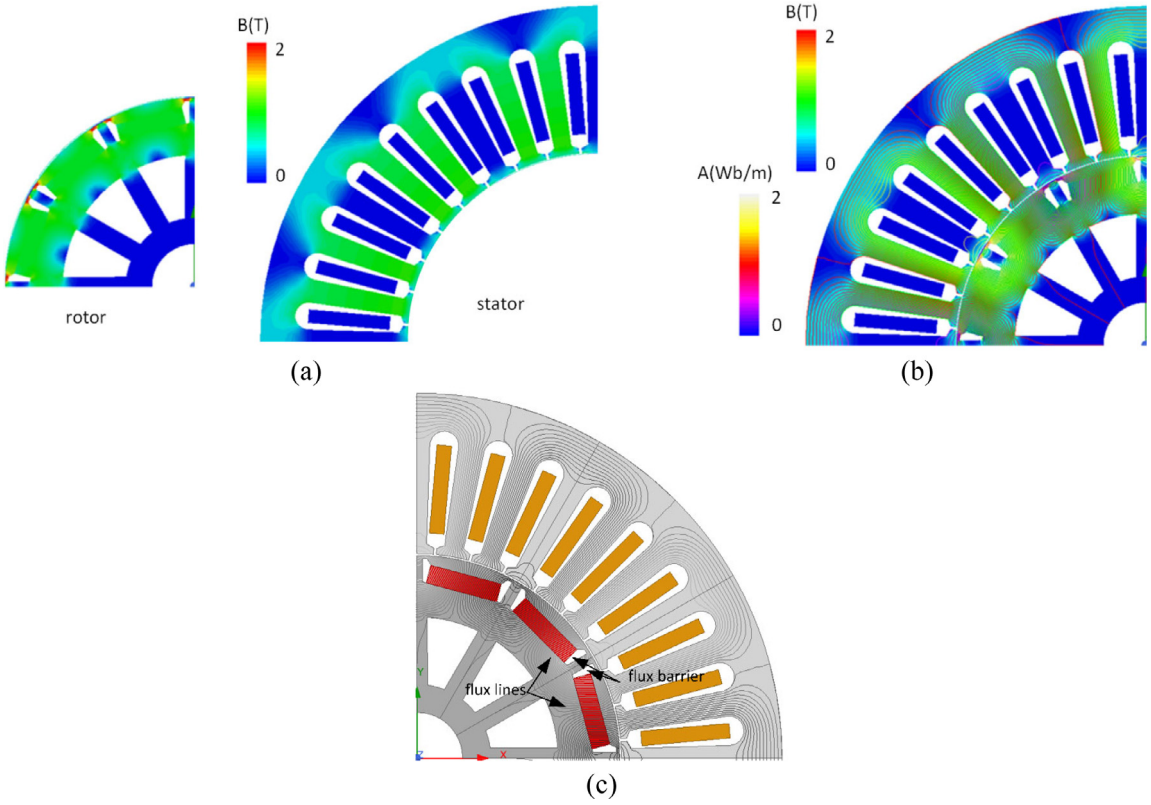

Fig. 8. Flux distribution and flux lines in different parts, (a) flux density, (b) flux lines, (c) effect of flux barrier on the flux distribution.

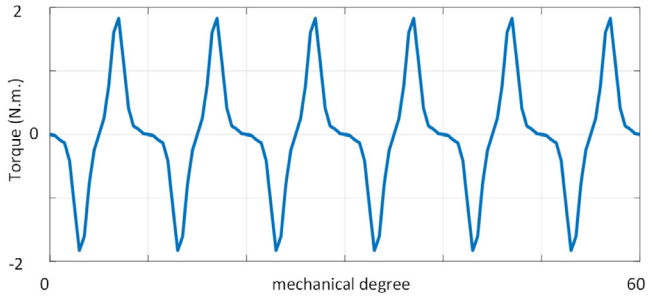

Fig. 9. Cogging torque.

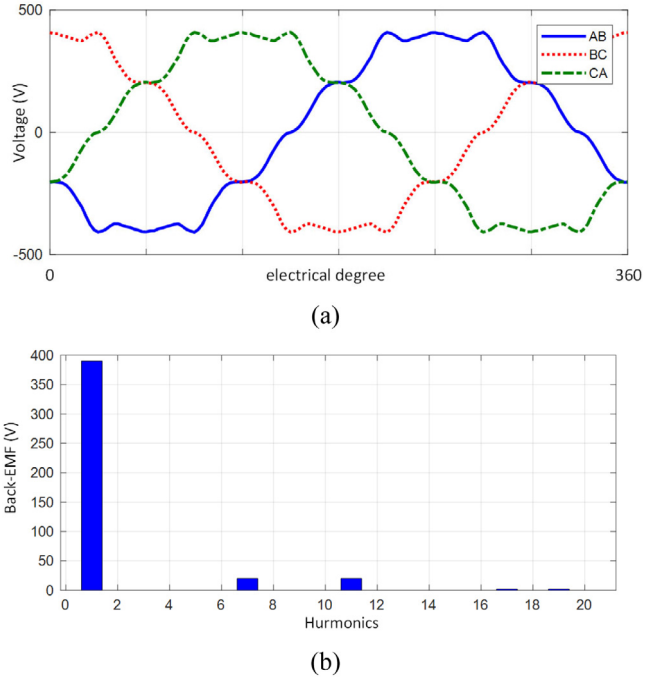

Fig. 10. No load induced voltage, (a) line voltages, (b) harmonics content.

4. Conclusion

The analytical design equations are suitable to find different design variants based on the specific output parameters. In this paper, the magnetic equivalent circuit has been used to extract the design equation for a radial flux PM generator that is used in direct drive wind power generation system. PM generators are one of the most interesting candidates for direct drive and high power density applications. The design method and equations could be extended to similar topologies and applications. Moreover, finite element analysis is used as the simulation tool for performance analysis of the designed generator. The peak to peak value of the output voltage is 640 V and the output torque is 19.1 N.m. as specified in the initial generator specifications. Sensitivity analysis shows that the smaller air-gap length increases the produced output voltage but, the PM thickness has no significant effect on the output characteristics. Simulation results show that the final design can satisfy the initial requirements that are determined based on the wind power generation system.

Declaration of competing interest

The authors declare that they have no known competing financial interests or personal relationships that could have appeared to influence the work reported in this paper.

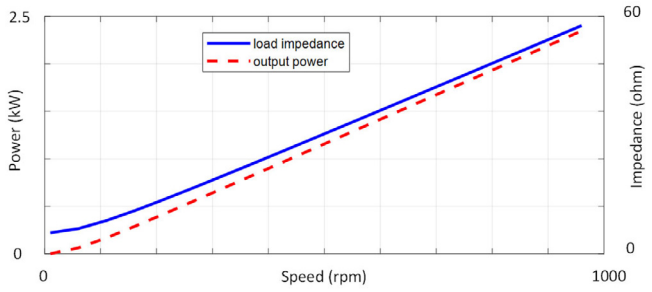

Fig. 11. Output power characteristics.

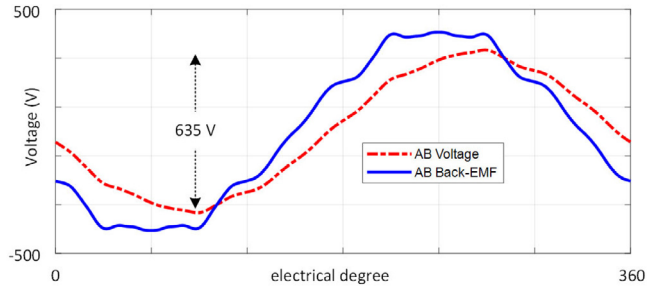

Fig. 12. Output voltage.

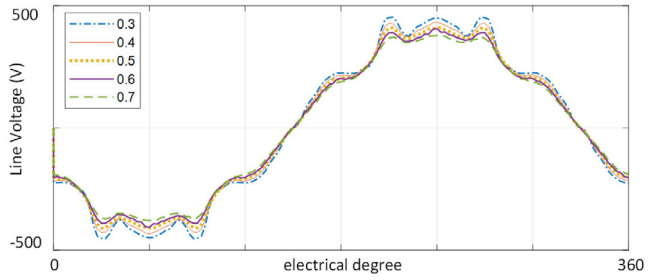

Fig. 13. Output line voltage for different air-gap lengths (mm).

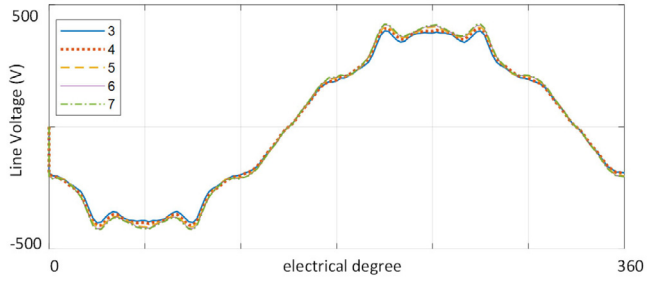

Fig. 14. Output line voltage for different PM thickness (mm).

References

Alhmoud, L., Wang, B., 2018. A review of the state-of-the-art in wind-energy reliability analysis. Renew. Sustain. Energy Rev. 81, 1643–1651.

Chen, Q., Eduku, S., Zhao, W., 2020. A new fault-tolerant switched flux machine with hybrid permanent magnets. CES Trans. Electr. Mach. Syst. 4 (2).

Chowdhury, A., Sozer, Y., 2020. Design and analysis of a hook shaped stator core with ring winding transverse flux machine for wind turbine applications. In: 2020 IEEE Energy Conversion Congress and Exposition (ECCE).

Şahin, A.D., Dincer, I., Rosen, M.A., 2006. Thermodynamic analysis of wind energy. Int. J. Energy Res. 30 (8), 553–566.

Dincer, I., Acar, C., 2015. A review on clean energy solutions for better sustainability. Int. J. Energy Res. 39 (5), 585–606.

Dobzhanskyi, O., et al., 2019. Axial-flux PM disk generator with magnetic gear for oceanic wave energy harvesting. IEEE Access 7, 44813–44822.

Du, Z.S., Lipo, T.A., 2017. Torque performance comparison between a ferrite magnet vernier motor and an industrial interior permanent magnet machine. IEEE Trans. Ind. Appl. 53 (3).

Elizondo, J., Martínez, J., Probst, O., 2009. Experimental study of a small wind turbine for low-and medium-wind regimes. Int. J. Energy Res. 33 (3), 309–326.

Feng, Y., Li, F., Huang, S., Yang, N., 2018. Variable-flux outer-rotor permanent magnet synchronous motor for in-wheel direct-drive applications. Chin. J. Electr. Eng. 4 (1).

Gao, Y., Qu, R., Li, D., Chen, F., 2017. Force ripple minimization of a linear vernier permanent magnet machine for direct-drive servo applications. IEEE Trans. Magn. 53 (6).

Gieras, J.F., 2002. Permanent Magnet Motor Technology: Design and Applications. CRC Press.

Hanselman, D.C., 2003. Brushless permanent magnet motor design. The Writers' Collective.

Hong, C., Huang, W., Hu, Z., 2018. Parameters and performance analysis of a dual stator composite rotor axial flux induction motor by an analytical method. IET Electr. Power Appl. 12 (8), 1158–1165.

Husain, T., et al., 2018. Design considerations of a transverse flux machine for direct-drive wind turbine applications. IEEE Trans. Ind. Appl. 54 (4), 3604–3615.

Jeong, C.L., Kim, Y.K., Hur, J., 2019. Optimized design of PMSM with hybrid-type permanent magnet for improving performance and reliability. IEEE Trans. Ind. Appl. 55 (5).

Li, K., Bouscayrol, A., Cui, S., Cheng, Y., 2021a. A hybrid modular cascade machines system for electric vehicles using induction machine and permanent magnet synchronous machine. IEEE Trans. Veh. Technol. 70 (1).

Li, W., Cheng, M., 2020. Investigation of influence of winding structure on reliability of permanent magnet machines. CES Trans. Electr. Mach. Syst. 4 (2).

Li, J., Lu, Y., Cho, Y.H., Qu, R., 2019. Design, analysis, and prototyping of a water-cooled axial-flux permanent-magnet machine for large-power direct-driven applications. IEEE Trans. Ind. Appl. 55 (4).

Li, X., Wang, X., Yu, S., 2021b. Design and analysis of a novel transverseflux tubular linear switched reluctance machine for minimizing force ripple. IEEE Trans. Transp. Electr. 7 (2).

Liang, J., Jiang, J.W., Yang, Y., Al-Ani, D., et al., 2019. Torque ripple reduction for interior permanent magnet synchronous machines under load excitation by optimizing rotor skew angles, In: 2019 23rd International Conference on Mechatronics Technology (ICMT).

Nasiri-Zarandi, R., Ajamloo, A.M., Abbaszadeh, K., 2020. Design optimization of a transverse flux Halbach-array PM generator for direct drive wind turbines. IEEE Trans. Energy Convers. 35 (3), 1485–1493.

Pyrhonen, J., Jokinen, T., Hrabovcova, V., 2013. Design of Rotating Electrical Machines. John Wiley & Sons.

Shen, Y., Shi, T., Lu, Q., Xia, C., 2021. Robust design and analysis of asymmetric-excited flux reversal PM linear machine for long-stroke direct drive propulsion. IEEE Trans. Magn. 57 (6).

Yang, X., et al., 2020. A novel dual-consequent-pole transverse flux motor and its analytical modeling. IEEE Trans. Ind. Electron. 68 (5), 4141–4152.

Yazdanpanah, R., 2020. Analytical study, design and optimization of radial-flux PM limited-angle torque motors. Sci. Iran. Accepted Manuscript. Available Online from 03 August 2020.

Yazdanpanah, R., Farjah, E., 2021. Analytical study on the cogging torque in surface-mounted PM machines; effect of armature notches and PM segments. Int. J. Appl. Electromagn. Mech. 65 (3), 487–500.

Yazdanpanah, R., Mirsalim, M., 2014. Hybrid electromagnetic brakes: design and performance evaluation. IEEE Trans. Energy Convers. 30 (1), 60–69.

Zhang, P., Lu, D., Salem, S., 2017. Electrical signature analysis based condition monitoring and diagnostics techniques for wind turbines, In: 2017 IEEE 11th International Symposium on Diagnostics for Electrical Machines, Power Electronics and Drives (SDEMPED), IEEE.

Zhao, X., Niu, S., Fu, W., 2019. Sensitivity analysis and design optimization of a new hybrid-excited dual-PM generator with relieving-DC-saturation structure for stand-alone wind power generation. IEEE Trans. Magn. 56 (1), 1–5.

Zhao, W., Yang, Z., Liu, Y., Wang, X., 2021. Analysis of a novel surface-mounted permanent magnet motor with hybrid magnets for low cost and low torque pulsation. IEEE Trans. Magn. 57 (6).